



Frequency-Dependent Absorbing Boundary Implementations in 3D Finite Difference Time Domain Room Acoustics Simulations

Stephen Oxnard, Dean O'Brien, Jelle van Mourik and Damian Murphy
The Audio Lab, Department of Electronics, University of York, York, United Kingdom.

Summary

Finite Difference Time Domain room acoustics modelling provides accurate emulation of sound propagation within enclosed structures. Inclusion of frequency-dependent boundary conditions in such models facilitates emulation of realistic sound wave interaction with absorbing surface materials. These boundary conditions can be implemented by means of octave band modelling or digital impedance filter methods. This paper extends research in this area by comparing results obtained from these boundary modelling methods in terms of accuracy and required computational resources. Results show that octave band approaches achieve a higher degree of accuracy over the digital impedance filter method. However, in terms of simulation run times, the octave band model must make use of parallel computation architectures to realise a simulation time lower than the digital impedance filter model. Furthermore, the results presented inform routes of further study focussing on refinement of both methods to create an optimal, computationally efficient frequency-dependent boundary model.

PACS no. xx.xx.Nn, xx.xx.Nn

1. Introduction

Wave-based physical modelling paradigms, such as the Finite Difference Time Domain (FDTD) method, facilitate highly accurate simulation of sound propagation in space. As such, FDTD methods have received considerable attention in recent years as a means of room acoustic modelling [1, 2]. The main advantage of FDTD and similar techniques is that they allow direct solution of the wave equation and, therefore, preserve wave phenomena such as standing waves, diffraction and interference effects. This is in contrast to alternative, and more computationally efficient, ray-based geometric acoustic models that fail to accurately represent wave characteristics and are consequently accurate at high frequencies only. The accuracy of FDTD methods is offset by the computational resources required to simulate the models, especially for large room volumes and high audio sampling rates. This notable disadvantage may be somewhat alleviated by combining FDTD and high frequency geometric modelling to produce a hybrid simulation system [3] or by using parallel processing units to run portions of the FDTD scheme simultaneously [2, 4].

In order to render room impulse responses (RIRs) the spatial domain simulated by the FDTD scheme

must be appropriately terminated at the bounding surfaces. This leads to the requirement of boundary conditions that emulate sound wave reflection as encountered in reality. To date, numerous approaches to modelling sound wave/surface interaction have been devised in relation to the physical behavior of surface materials in reaction to incident pressure waves. In particular, the problem of representing frequency-dependent absorption at a boundary has gained considerable attention recently in order to create model surfaces that better match those encountered in practice. This work seeks to examine two different implementations of the frequency-dependent Locally Reacting Surface (LRS) boundary condition in FDTD schemes, as documented in [5]. The first implementation is an octave band approach that follows the procedure initially documented in [6]. An octave band model requires the model to be simulated for each contributing frequency band with respective absorption coefficients applied in each simulation. The second implementation makes use of the Digital Impedance Filter (DIF) boundary condition as presented in [7]. This approach emulates frequency-dependent absorption characteristics by filtering sound waves as they interact with a bounding surface to remove an appropriate amount of acoustic energy in each octave band in accordance with surface absorption properties. Both frequency-dependent boundary implementations have been examined in previous studies, how-

(c) European Acoustics Association

Table I. Overview of source and receiver placements defined for each RIR measurement.

CASE	Source (x,y,z) (m)	Receiver (x,y,z) (m)
1	(0.21, 0.21, 0.21)	(3.83, 2.77, 2.34)
2	(2.13, 1.49, 1.28)	(2.55, 2.77, 1.28)
3	(0.42, 1.50, 1.70)	(3.70, 0.42, 1.70)

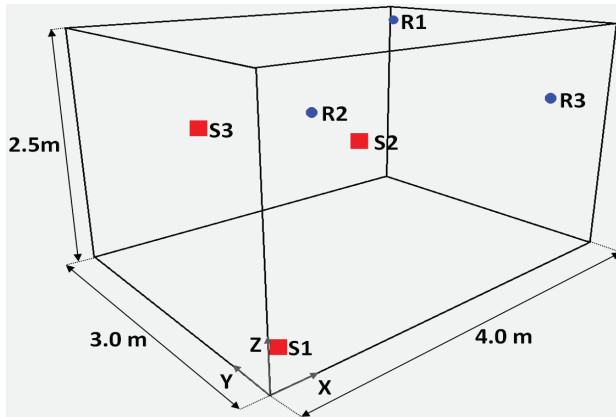


Figure 1. Overview of the case study room geometry. Dimensions, source positions (S1-S3) and receiver positions (R1-R3) are displayed.

ever a comparison in terms of analysis of resulting RIRs and computational requirements has not yet been conducted. In addition, the examination of the DIF boundary has so far been restricted to scenarios involving simple low order filters that are subject only to numerical analysis. The work presented in this paper seeks to expand on previous research by directly comparing the properties of RIRs rendered using the octave band and DIF boundary simulations for realistic surface materials.

2. Case Study Room Characteristics

The target acoustic environment selected for this work is a fully bounded cuboid topology. The choice of a simple room geometry enables modal analysis to compare resonant frequencies present in resulting RIRs and those calculated from known eigenvalue solutions of the wave equation in a rectilinear space.

The chosen room geometry consists of six bounding surfaces representing a floor and ceiling of side length 4 x 3 m and four vertical walls, 2.5 m in height. Three source and receiver locations are defined throughout the space as listed in Table I and depicted alongside the room topology in Figure 1. In the following, the source and receiver combinations will be referred to as case 1, 2 and 3 corresponding to Source/Receiver 1-3 respectively.

Materials, possessing frequency-dependent absorption characteristics, are defined for each surface of the room in two arrangements. In the first arrangement,

Table II. Summary of absorption (α) and reflection (R) coefficients for the materials applied to model surfaces for each octave band simulated.

Material	f_l :Center Frequency: f_u (Hz)	α	R
Plaster (Ceiling)	44 : 63 : 88	0.08	0.9592
	88 : 125 : 177	0.08	0.9592
	177 : 250 : 355	0.2	0.8944
	355 : 500 : 710	0.5	0.7071
	710 : 1k : 1.42k	0.4	0.7746
	1.42k : 2k : 2.84k 2.84k : 4k : 5.68k	0.4 0.36	0.7746 0.8000
Wood (Floor)	44 : 63 : 88	0.15	0.9920
	88 : 125 : 177	0.15	0.9920
	177 : 250 : 355	0.11	0.9434
	355 : 500 : 710	0.1	0.9487
	710 : 1k : 1.42k	0.07	0.9644
	1.42k : 2k : 2.84k 2.84k : 4k : 5.68k	0.06 0.06	0.9695 0.9695
Concrete (Walls)	44 : 63 : 88	0.02	0.9899
	88 : 125 : 177	0.02	0.9899
	177 : 250 : 355	0.03	0.9849
	355 : 500 : 710	0.03	0.9849
	710 : 1k : 1.42k	0.03	0.9849
	1.42k : 2k : 2.84k 2.84k : 4k : 5.68k	0.04 0.07	0.9798 0.9644

the absorption characteristics of a plasterboard material are applied consistently across all surfaces. The second arrangement includes a wooden floor, a plasterboard ceiling and rough concrete walls. Frequency-dependent absorption data for the three materials are based on data from [8] and are listed in octave bands in Table II. The absorption data takes the form of an absorption coefficient, α , that defines the ratio of ingoing and outgoing pressure of a sound wave upon reflection. This relates to the reflection coefficient as $R = \sqrt{1 - \alpha}$.

3. FDTD Acoustic Modelling

The formulation of the FDTD scheme utilised in this study begins with the 3D homogeneous wave equation for an ideal isotropic medium,

$$\frac{\partial^2}{\partial t^2} p(\mathbf{x}, t) = c^2 \nabla^2 p(\mathbf{x}, t) \quad (1)$$

where $p(\mathbf{x}, t)$ is the acoustic pressure at position $\mathbf{x} = [x, y, z]$ in 3D Cartesian space, c is wave speed in ms^{-1} , t is time in seconds and $\nabla^2 = \frac{\partial^2}{\partial x^2} + \frac{\partial^2}{\partial y^2} + \frac{\partial^2}{\partial z^2}$ is the 3D Laplacian operator. The wave speed is set to $344 ms^{-1}$ for all simulations. Application of second order accurate centered finite difference approximations facilitates discretisation of equation 1 and results in the 'Standard Rectilinear' (SRL) scheme (see e.g. [7]), which is applied to calculate pressure fluctuations in the interior of the cuboid domain.

To ensure numerical stability in simulations, a stability limit, derived through Von Neumann analysis [10] must be applied. This limit imposes a lower bound on the grid spacing in the discrete spatial domain h such that $h \geq \sqrt{3}ck$ where k is the discrete time step

(s). All simulations are conducted with h equal to this lower bound for maximum spatial resolution. In addition, it has been shown that dispersion error resulting from anisotropic wave propagation over the discretised SRL domain reduces the usable bandwidth of simulation results to $0.196 F_s$ [9]. Therefore, the FDTD models are simulated with a temporal sampling frequency of $\sim 5x$ the upper frequency limit of interest.

Room impulse responses are rendered by first exciting the acoustic model with a Kronecker delta function at the closest grid point to the source location in each RIR case. The pressure fluctuations are then recorded at the closest grid point to the respective receiver location producing an RIR for each source/receiver case.

4. FDTD Octave Band Boundary Model

The locally reacting surface (LRS) boundary condition [5] is applied to the bounding surfaces of the acoustic model. Boundaries of this kind enable direct application of reflection coefficients to surfaces in order to model material sound absorption characteristics encountered in practice. The LRS boundary condition takes the form,

$$\frac{\partial p}{\partial t} = -c\zeta \frac{\partial p}{\partial N}; \quad \zeta = \frac{1+R}{1-R} \quad (2)$$

after [5], where ζ is an impedance term related to an arbitrary material reflection coefficient, R , and N is the direction normal to the boundary. In most cases and for the purposes of this study, R is assumed to lie in the range $[0,1]$ giving a phase-preserving boundary. The condition in equation 2 is inserted into the update equations for all grid points on the bounding surfaces of the acoustic model enabling the reflection of each surface to be controlled. A detailed derivation of LRS boundaries and their implementation in 3D FDTD schemes is presented in [7]. Following the procedure documented in [6], two approaches to LRS octave band simulation are devised.

4.1. Constant F_s Octave Band Modelling

As noted in section 2, the highest required frequency to be simulated in the acoustic model is the upper cut-off frequency of the 4 kHz octave band, 5680 Hz. To avoid numerical dispersion effects, a sampling frequency of $F_s = 28400$ Hz is selected for simulations. The acoustic model is then simulated for each of the 7 octave bands with respective reflection coefficients in turn, capturing RIRs for the 3 pre-defined source and receiver cases. The RIRs are then grouped according to the source/receiver case and passed through a band-pass filter bank composed of zero-phase, 3rd order Butterworth filters. The purpose of the band-pass

Table III. Sampling rates applied to each octave band model for the variable F_s approach. The maximum error in model dimensions is also provided.

Octave Band (Hz)	F_s (Hz)	Max. Dimension Error (%)
63, 125, 250	2800	2.14
500	3700	3.06
1000	7100	0.70
2000	14200	0.70
4000	28400	0.18

filter bank is to isolate the frequency range (or octave) which corresponds to the reflection coefficient applied during simulation. The total RIR in each case is created by summing the filtered octave band contributions. Finally, a DC blocking filter is applied to each RIR to remove DC offset drift introduced by the Kronecker delta excitation function. This process is repeated for the two material arrangements defined in section 2.

4.2. Variable F_s Octave Band Modelling

For the variable F_s models, each octave band is simulated with the temporal sampling rate set sufficiently high to simulate the required bandwidth while avoiding dispersion effects. It is necessary to impose a lower sampling rate limit for the lowest 3 octave band (63, 125, 250 Hz) models in order to maintain geometry specific consistency between all octave band models. The sampling rates listed in Table III ensure that model geometries are within a maximum error of 3.1% in all dimensions and source and receiver locations deviated by a maximum of 0.11 m from the specified position. The maximum deviation in terms of source and receiver locations occurs for RIR case 2 in the 500 Hz octave band. Prior to applying the filter bank to the collected RIRs, each RIR requires calibration to ensure that the energy of adjacent octave band contributions are equalised across the frequency spectrum as noted in [11]. Following the procedure documented in [11], each RIR is multiplied by a weighting coefficient, K , defined as:

$$K = \frac{\lambda F_s}{p_{DC} c} \quad (3)$$

where p_{DC} is the DC component of the RIR to which the weighting is being applied. It is then necessary to upsample the 63 - 2000 Hz octave band RIRs to the sampling rate of the highest octave band, $F_s = 28400$ Hz. Having conducted these calibrations, it is then possible to apply the band-pass filter bank used in the constant F_s approach to the results creating the total RIRs.

5. FDTD DIF Boundary Model

The digital impedance filter boundary may be used to create a frequency-dependent version of the LRS

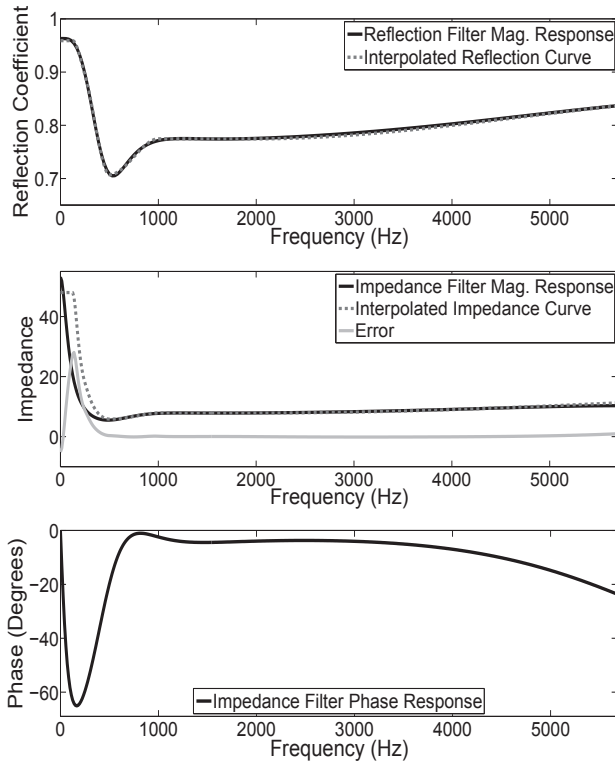


Figure 2. [Top to Bottom]: The reflection filter magnitude response and the ideal reflection curve for the plasterboard material; resulting impedance filter magnitude response, the ideal impedance curve and the difference (Error) between the two; phase response of the plasterboard impedance filter.

boundary condition. As such, the DIF model requires only one simulation to render RIRs across the entire frequency bandwidth. The implementation of this approach stems from extension of the impedance-reflection relation given in equation 2. Instead of defining a single reflection coefficient, the reflection may be expressed as a function of frequency with its value varying as required for each octave band. This function is then used to define a filter transfer function culminating in the design of a reflection filter $R(z)$. It follows (see e.g. [7]) that the related impedance filter may be defined using:

$$\zeta(z) = \frac{1 + R(z)}{1 - R(z)} \quad (4)$$

which implies that the impedance filter relies on the creation of a suitable reflection filter.

For the purposes of this study, three IIR reflection filters are designed to represent the variance of reflection over frequency for each surface material defined in Table II. Each filter transfer function is created by interpolating the required reflection coefficients for each octave band and using the result as the magnitude response of the filter. This magnitude response is passed into the MATLAB Signal Processing Toolbox function `fdesign.arbmag` which yields the filter

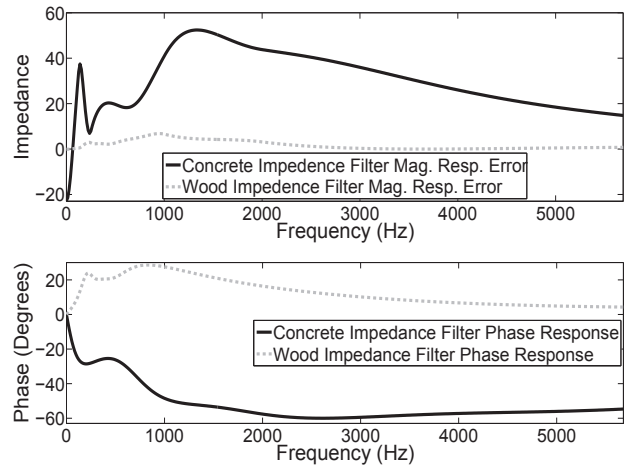


Figure 3. [Top to Bottom]: The difference (Error) between the ideal impedance curve and the resulting impedance filter magnitude response for the concrete and wood material filters; phase response of the concrete and wood impedance filters.

coefficients required for the given response and a predefined filter order. Having calculated the coefficients of the filter function $R(z)$, it is then possible to calculate the impedance filter transfer function $\zeta(z)$ using equation 4.

Figure 2 shows the magnitude responses of both the reflection and impedance filters designed to represent the plasterboard material properties. The agreement between the interpolated reflection curve and the reflection filter is shown to be reasonable. This magnitude response required a 12th order filter and increasing the filter order was found to have negligible impact on the level of accuracy. However, small discrepancies between desired and designed reflection magnitude curves impact significantly on the accuracy of the resulting impedance filter as shown in the middle panel of Figure 2. The difference between the ideal response and the filter magnitude response is displayed as an error calculated by subtracting the filter response from the interpolated curve. It is evident that the impedance filter response is not ideal in the frequency range 0 - 500 Hz. In addition, the impedance filter has a highly non-linear phase response for frequencies less than 1 kHz. The impact of these filter design issues is examined in section 6. The remaining two impedance filters representing the wood and concrete materials are of 14th and 18th order respectively. For brevity, their associated transfer functions are displayed in terms of the error between the required and actual magnitude response curves and phase responses in Figure 3. As displayed, the magnitude of the filter representing concrete exhibits large error in the frequency range 0 - 2 kHz. This deviation is again due to small errors in the reflection filter response which become magnified in the resulting impedance filter magnitude curve. The error observed in the wood impedance filter is less pronounced and

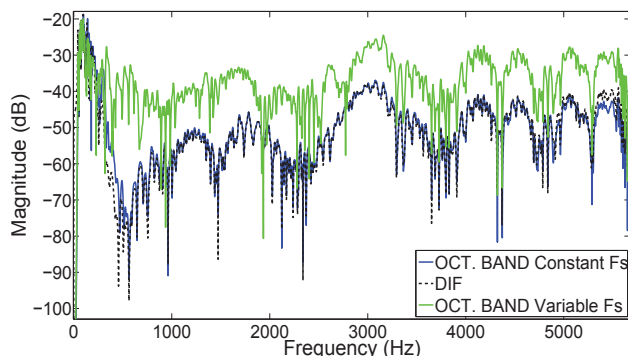


Figure 4. Spectra of RIRs rendered using each modelling method for RIR case 1 and material arrangement 1.

both filters have non-linear phase responses in low to mid frequencies.

The DIF boundary is implemented for each RIR case and for both material arrangements following the procedure outlined in [7]. In total, 6 RIRs were rendered using the DIF boundary: material arrangement 1 (plasterboard material assigned to all surfaces), RIR cases 1-3; material arrangement 2 (plasterboard ceiling, wood floor and concrete walls), RIR cases 1-3.

6. Results and Discussion

In summary, a total of 6 RIRs were rendered using each of the 3 boundary modelling approaches corresponding to 3 RIR cases and 2 material arrangements. Audio examples of resulting RIRs are available on the supporting website for this paper [12].

6.1. Frequency Domain Analysis

Analysis of the magnitude spectra of the rendered RIRs is the optimal means of evaluating the correctness of the model simulations. Firstly, this allows visual inspection of the relative energy levels across each frequency band modelled to verify that results agree with the frequency-dependent absorption values applied to the room surfaces in each arrangement. Secondly, modal analysis can be applied.

Figure 4 depicts the comparison between all three modelling methods for RIR case 1 and material arrangement 1. It is clear that the calibration method applied to the variable F_s octave band model produces a sizable magnitude offset. This is discerned from the upper 4 kHz octave band, where, the RIR produced is equal to that of the constant F_s octave band model. However, the shape of the octave band model responses in the 4 kHz band is highly comparable. At low frequencies, the similarity of the octave band results becomes less apparent. This result was evident in all RIR cases for both material arrangements. The cause of these significant differences between constant and variable F_s octave band RIRs will be examined in future work.

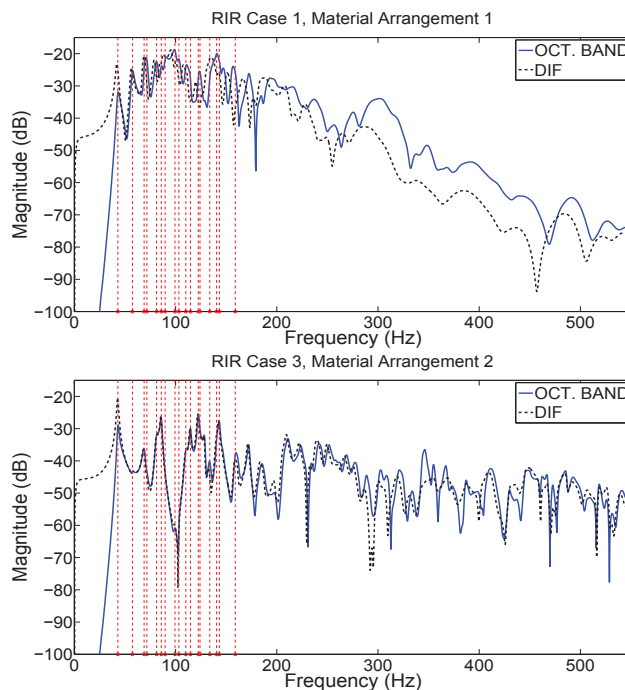


Figure 5. [Top to Bottom]: Low frequency spectra of constant F_s octave band and DIF boundary models. RIR cases and material arrangements are noted and theoretical modal frequencies are given by the vertical lines.

The similarity between the DIF and constant F_s octave band RIRs across the entire modelled bandwidth is striking. The RIR spectra demonstrate correct absorption characteristics for the plasterboard material assigned throughout the model. Figure 5 (top panel) displays the same RIR magnitude spectra up to 550 Hz and theoretical low order modal values. This diagram highlights the impact of the discrepancy between the impedance filter response curve and the impedance values applied in the octave band model (see Figure 2). The octave band RIR shows good agreement with theoretical modal values whereas the the DIF model RIR exhibits a slight shift in resonant frequencies. This shift may be attributed to the phase response of the impedance filter highlighted in Figure 2. This result draws attention to the fact that the phase response of the filter must be linear in order to maintain correct modal resonances in the DIF boundary model. The effect of the impedance filter phase response is also clear from the lower diagram in Figure 5 that shows the DIF and octave band model RIRs for case 3 and material arrangement 2. Both RIRs show good agreement with low order modal values. However, as frequency increases, the phase delay of the contributing impedance filters (see Figures 2 & 3) has an increasing impact on the positioning of resonant peaks in the spectra of the DIF model RIR. In summary, the agreement between octave band and DIF boundary simulation results is highly dependent on the characteristics of the impedance filters applied in the DIF boundary model. These characteristics are,

in turn, sensitive to the design of the respective reflection filters implying that the indirect construction of the impedance filters is not advisable. Hence, it can be concluded that the constant F_s boundary model is the most reliable approach in terms of RIR accuracy.

6.2. Simulation Data

The run time and required number of grid points of all simulations carried out in this study are summarised in Table IV. Run times relate to the simulation time for 1 second of RIR output.

Table IV. Run time and number of grid points (nodes) used for each model simulation. Memory requirements for floating-point precision simulations is also provided.

Model	Band (Hz)	F_s	Nodes	Run time (s)	Mem. (MB)
OB VF_s	63, 125, 250	2800	11700	0.03	0.09
OB VF_s	500	3700	26520	0.12	0.20
OB VF_s	1000	7100	168609	1.33	1.29
OB VF_s	2000	14200	1264896	26.93	9.65
OB C/VF_s	4000	28400	9953280	429.23	79.54
DIF MA1	[ALL]	28400	16669440	1670.00	127.18
DIF MA2	[ALL]	28400	17691072	2014.00	135.00

Key: OB VF_s - Octave Band Variable F_s , OB C/VF_s - Octave Band Constant and/or Variable F_s , DIF MA1 - DIF model, material arrangement 1, DIF MA2 - DIF model, material arrangement 2.

The variable F_s octave band model requires the smallest run time and memory requirements in terms of the number of required grid points. Sequentially, the variable octave band model may be simulated in approximately 456 seconds reducing run times by $\sim 5x$ compared to sequential simulation of the constant F_s model. In addition, a parallel implementation of the variable F_s model achieves a reduction of memory requirement of 310 MB against a parallel constant F_s octave band simulations. However, as demonstrated previously, this saving comes at the cost of notable inaccuracies in results which will become the focus of future research in order to capitalise on the computational savings.

The DIF model is shown to require over 1.5x the number of grid points required by each model in the constant F_s octave band model in order to facilitate the high-order filters applied at each boundary node. This increase in number of grid points causes a large increase in memory requirements ($\sim 48 - 66$ MB) that is proportional to the order of the boundary filters applied. The run times recorded suggest that the DIF model is computationally more efficient than sequential constant F_s octave band simulations. With reference to the results recorded to date, a parallel implementation of the constant F_s octave band model provides an optimum approach to frequency-dependent boundary modelling both in terms of simulation run time and accuracy of results.

7. Conclusions

The studies in this paper have examined the comparison of three frequency-dependent boundary implementations in FDTD schemes. Comparative examination of RIRs simulated in each model demonstrate that constant F_s octave band boundary modelling produces optimal results in terms of RIR accuracy, but requires parallel computation in order to achieve lower run times than the DIF model. Future work will focus on refinement of the DIF and variable F_s methods to improve result accuracy and capitalise on run time savings.

References

- [1] J. Sheaffer, B. Fazenda, "WaveCloud: an open source room acoustics simulator using the finite difference time domain method," *Proc. of Forum Acusticum*, Krakow, Poland, Sept. 2014.
- [2] C. Webb, S. Bilbao, "Computing Room Acoustics with CUDA - 3D FDTD schemes with boundary losses and viscosity," *Proc. of the IEEE Int. Conf. on Acoustics, Speech and Language Processing (ICASSP)*, Prague, Czech Republic, May 2011.
- [3] A. Southern, S. Siltanen, D. T. Murphy, L. Savioja, "Room Impulse Response Synthesis and Validation Using a Hybrid Acoustic Model," *IEEE Transactions on Audio, Speech, and Language Processing*, Vol. 21, No. 9, pp. 1940-1952, Sept. 2013.
- [4] L. Savioja, "Real-Time 3D Finite-Difference Time-Domain Simulation of Low- and Mid-Frequency Room Acoustics," *Proc. of the 13th Int. Conf. on Digital Audio Effects (DAFx-10)*, Graz, Austria, Sept. 2010.
- [5] K. Kowalczyk, M. van Walstijn, "Formulation of a locally reacting wall in finite difference modelling of acoustic spaces," *Int. Symp. on Room Acoustics (ISRA)*, Seville, Spain, Sept. 2007.
- [6] J. Sheaffer, B. M. Fazenda, D. T. Murphy, J. A. S. Angus, "A simple multiband approach for solving frequency dependent problems in numerical time domain methods," *Proc. of Forum Acusticum*, Aalborg, Denmark, Jun. 2011.
- [7] K. Kowalczyk, M. van Walstijn, "Modelling frequency-dependent boundaries as digital impedance filters in FDTD and K-DWM room acoustic simulations," *J. Audio Eng. Soc.*, vol. 56, No. 7/8, pp. 569-583, Jul./Aug., 2008.
- [8] ODEON Website, Last Accessed 27th Feb. 2015 [online], Available: <http://www.odeon.dk>
- [9] K. Kowalczyk, M. van Walstijn, "Room acoustics simulation using 3-D compact explicit FDTD schemes," *IEEE Transactions on Audio, Speech, and Language Processing*, Vol. 19, No. 1, pp. 34-46, Jan. 2011.
- [10] A. Taflov, S. C. Hagness, *Computational Electrodynamics: The Finite-Difference Time-Domain Method*, 2nd ed. (Artech House, Norwood, MA, 2000).
- [11] S. Siltanen, A. Southern, L. Savioja, "Finite-Difference time domain method source calibration for hybrid acoustics modeling," *Proc. of the IEEE Int. Conf. on Acoustics, Speech and Signal Processing (ICASSP)*, Vancouver, Canada, May 2013.
- [12] Supporting Website, Last Accessed 27th Feb. 2015 [online], Available: <http://www-users.york.ac.uk/~so523/EuroNoise.html>